MPC-based 3-D trajectory tracking for an autonomous underwater vehicle with constraints in complex ocean environments

Yongding Zhang [a,b], Xiaofeng Liu [c,d,e,*], Minzhou Luo [e], Chenguang Yang [f]

[a] College of Computer and Information, Hohai University, Nanjing 210098, China
[b] School of Computer and Information Engineering, Chuzhou University, Chuzhou 239000, China
[c] College of IoT Engineering, Hohai University, Changzhou 213022, China
[d] Changzhou Key Laboratory of Robotics and Intelligent Technology, Changzhou 213022, China
[e] Jiangsu Key Laboratory of Special Robots (Hohai University), Changzhou 213022, China
[f] Bristol Robotics Laboratory, University of the West of England, Bristol, BS16 1QY, UK

ARTICLE INFO

ABSTRACT

This paper presents a novel three-dimension (3-D) underwater trajectory tracking method for an autonomous underwater vehicle (AUV) using model predictive control (MPC). First, the 6-degrees of freedom (DoF) model of a fully-actuated AUV is represented by both kinematics and dynamics. After that, the trajectory tracking control is proposed as an optimization problem and then transformed into a standard convex quadratic programming (QP) problem which can be readily computed online. The practical constraints of the system inputs and states are considered effectively in the design phase of the proposed control strategy. To make the AUV move steadily, the control increments are considered as the system input and optimized. The receding horizon implementation makes the optimal control inputs be recalculated at each sampling instant, which can improve the robustness of the tracking control under the model uncertainties and time-varying disturbances. Simulations are carried out under two different 3-D trajectories to verify the performance of trajectory tracking under random disturbances, ocean current disturbances, and ocean wave disturbances. The simulation results are given to show the feasibility and robustness of the MPC-based underwater trajectory tracking algorithm.

1. Introduction

As tools for human beings to explore and develop the ocean, autonomous underwater vehicles (AUVs) have drawn a lot of attention from researchers around the world (Xiang et al., 2015). Over the past few decades, AUVs have been increasingly used in scientific, industrial, commercial and military areas. The main applications include oceanographic mapping, deep sea exploration (Zhang et al., 2015), offshore oil and gas development, pipeline maintenance (Xiang et al., 2010), maritime rescue, underwater target tracking (Ferri et al., 2018) and patrolling (Zhang et al., 2007). In order to execute above tasks well, it is necessary to implement precise control for AUVs (Refsnes et al., 2008; Kim et al., 2016). However, it is a hard task to accurately control the AUVs because of the model nonlinearity, complex hydrodynamic coefficients and uncertain external disturbances (Cui et al., 2016). That is why the motion control of the AUVs attracts a lot of attention from researchers worldwide.

Trajectory tracking is the main technical basis for AUVs to perform various underwater tasks, which involves the design of a controller so that the AUVs can follow a desired, time-parameterized trajectory starting from a given initial state (either on or off the trajectory) (Aguiar and Hespanha, 2007; Wang et al., 2017). Over the past several decades, many kinds of control methods have been proposed to tackle the trajectory tracking problem, such as proportional–integral–derivative (PID) control, backstepping control (BSC), adaptive control, fuzzy logic control (FLC), sliding mode control (SMC), neural network control (NNC) and model predictive control (MPC) (Khodayari and Balochian, 2015; Xiang et al., 2017; Qiao et al., 2017; Zhu et al., 2018; Gan et al., 2018; Peng et al., 2019b). PID is a simple control method with low complexity. In Jalving (1994), a PID-based control system was proposed and three autopilots were designed for steering, heaving and velocity control. In Perrier and Canudas-De-Wit (1996), a PID controller for subsea robots was introduced, which could address the linear constraint caused by the low sampling rate. However, PID can provide accurate control only if the system model is linear and the interferences are constant (Smallwood and Whitcomb, 2004). BSC has been a useful method to control nonlinear systems. In Xu et al. (2014),

---

a BSC controller was proposed, which defined a virtual speed error dynamics and could effectively avoid the problem of singularity and simplify the calculations. A BSC-based 3D trajectory tracking method was designed for underactuated AUVs, in which the velocity error function was constructed to obtain the proper control force and moments (Ye et al., 2015). However, the computing complexity increases rapidly as the system order increases because of the repeated differentiations of virtual controllers (Park et al., 2010). The adaptive control method is presented for plants with uncertain dynamics. In Antonelli et al. (2001), an adaptive approach was proposed for AUVs in the complex underwater environment where the parameters are dynamic and difficult to obtain. Sahu and Subudhi (2014) proposed an adaptive controller for underwater vehicles, in which the hydrodynamic effects was considered. However, the adaptive control method is effective only for the system with constant or slow changing parameters, and the complexity grows drastically as the system order increases (Xu et al., 2015). SMC is a promising control method for accurate trajectory tracking due to its strong robustness against uncertain model and time-varying parameters. In Londhe et al. (2017), a SMC method based on an uncertainty disturbance estimator was presented, which could effectively compensate the hydrodynamic uncertainty and unknown disturbances of an AUV. In Qiao and Zhang (2019a), a second-order fast nonsingular terminal SMC method was proposed for the trajectory tracking of fully actuated AUVs in the presence of dynamic uncertainties and time-varying external disturbances. A double-loop integral terminal SMC scheme was designed, which could improve the tracking accuracy and enhance the robustness against parameter uncertainties (Qiao and Zhang, 2019b). However, the SMC method may incur an undesirable high-frequency oscillations called "chattering" around the sliding surface, which can lead to low control accuracy and high energy consumption (Hammad et al., 2017). FLC is an intelligent control method which can make machines reason like humans. A robust fuzzy inference system was introduced for AUV docking, which used the fuzzified command and velocity vector fields to control the vehicle (Teo et al., 2012). In Sun et al. (2018), a fuzzy control method was introduced for AUV mission in the complex underwater environment, which can obtain an optimal path by incorporating with an optimization algorithm. However, FLC needs existing experience to establish fuzzy rules which is very subjective (Gan et al., 2018). NNC utilizes a neural network as controller, which can approximate any nonlinear function (Peng et al., 2019a). A robust nonlinear controller for AUVs was introduced to approximate the uncertain dynamics based on a linearly parameterized neural network (Ji et al., 2007). Park (2015) proposed a tracking control method based on the neural network to cope with the model uncertainties of AUV. The main disadvantage of NNC is that it has large computation cost and weak real-time performance (Gan et al., 2018). There are still some weaknesses of the aforementioned trajectory tracking methods, for instance, the input and state constraints are hardly to be dealt with conveniently. Ignoring the system constraints during the design stage may lead to poor performances of the trajectory tracking.

MPC is a closed-loop optimal control strategy which can provide a systematic way to deal with the input and state constraints. The system constraints caused by physical or security restrictions widely exist in all control systems. In Beal and Gerdes (2013), a MPC controller was utilized to bound the vehicle motion within a stable region of the state space. In Gao et al. (2016), a nonlinear MPC-based adaptive positioning control approach for an underwater vehicle was presented, in which the MPC controller are combined with a neural network adaptive controller to achieve the tracking optimization and improve the robustness to model uncertainty and unknown dynamics. A standard MPC framework for AUV trajectory tracking was proposed to overcome the problem of strong model non-linearity and a contraction constraint was considered to theoretically guarantee the stability of closed-loop system (Shen et al., 2017, 2018). However, the authors only designed some simple simulations without any interferences.
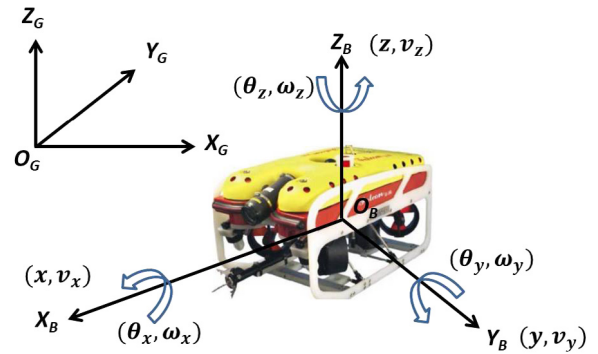

Fig. 1. Reference frames, AUV image courtesy of http://seaeye.com.

In this paper, the analysis of trajectory tracking problem for an AUV is conducted, and a MPC-based 3-D trajectory tracking method is presented. The input and state constraints are explicitly considered in the algorithm. The trajectory tracking problem is transformed into an optimization problem with input and state constraints. The state constraints are transformed into a form of input constraints and then the optimization problem is transformed into a standard quadratic programming problem which can be computed online. When the AUV reaches a new position, the next optimal inputs are recalculated based on the current states and the desired trajectory. Therefore, the MPC-based algorithm can still be carried out well even in the complex ocean environment with several uncertain disturbances. At last, the trajectories used for the illustration during simulations are a raster scan path and a sinusoidal curve. Simulation results are presented and discussed which verify the effectiveness and robustness of the designed tracking control method.

The rest of this paper is organized as follows. Section 2 presents the reference frames and mathematical model used for AUV trajectory tracking. In Section 3, the formulation of the optimization problem is introduced and the detailed MPC design procedure is formulated. Simulation results of the MPC-based method are illustrated in Section 4. Finally, conclusive remarks of this paper are given in Section 5.

2. AUV modeling

2.1. Frames of reference

The AUV motion is generally described in 6-degrees of freedom (DOF) which includes translational component and rotational component. The translational component includes surge, sway and heave, which describe the AUV's position. The rotational component consists of roll, pitch and yaw, which describe the AUV's orientation. In order to study the motion model, an AUV can be regarded as a rigid body in 3-D space.

For the convenience of clearly analyzing the 6-DOF motion of AUV, as depicted in Fig. 1, an inertial reference frame (i-frame) and a body-fixed frame (b-frame) are defined. The i-frame, which is denoted by (O_G, X_G, Y_G, Z_G), is coincident with the East-North-Up (ENU) coordinate system in this paper. Within this frame, origin O_G is a point on the surface of the ocean, the X_G-axis points towards the east, the Y_G-axis points towards the north, and the Z_G-axis points upwards perpendicular to the Earth's surface. The b-frame is a moving reference frame denoted by (O_B, X_B, Y_B, Z_B), the origin O_B of which coincides with the center of the AUV gravity. The X_B-axis is directed from aft to fore along the longitudinal axis of the AUV, the Y_B-axis points towards larboard, and the Z_B-axis is directed from bottom to top.

2.2. Kinematic model

The i-frame is used to record the global information of the AUV motion. Therefore, the motion of AUV need to be described as the motion of the b-frame with respect to the i-frame. In this paper, the Euler angle parameterization is used to describe the transformations between the two frames. As depicted in Fig. 1, the orientation of the b-frame with respect to the i-frame is expressed in terms of three successive rotations about the axes Z_B, Y_B and X_B, which are yaw ϕ_z, pitch ϕ_y, and roll ϕ_x, respectively.

Let $s_1 = [x, y, z]^T$ and $s_2 = [\phi_x, \phi_y, \phi_z]^T$ be the position vector and orientation vector of the AUV in the i-frame, where x, y and z represent the three Cartesian coordinates, ϕ_x, ϕ_y and ϕ_z represent the three attitude components (roll, pitch, and yaw angles), respectively. In order to avoid the singularity problem of the Euler angle, the pitch angle ϕ_y is bounded, satisfying $-\pi/2 < \phi_{y_{min}} \leq \phi_y \leq \phi_{y_{max}} < \pi/2$, where $\phi_{y_{min}}$ and $\phi_{y_{max}}$ represent the predefined lower bound and upper bound of ϕ_y, respectively. In practice, the pitch angle is not likely to get close to $\pi/2$ because of the metacentric restoring forces (Do and Pan, 2009). As a result, the constraint of ϕ_y is reasonable. Furthermore, let $v_1 = [v_x, v_y, v_z]^T$ and $v_2 = [\omega_x, \omega_y, \omega_z]^T$ be the linear velocity vector and angular velocity vector of the AUV in the b-frame, where v_x, v_y, v_z are the three translational velocity components, and ω_x, ω_y, ω_z are the three rotational velocity components, respectively. With these notations, the linear velocity vector $\dot{s}_1$ along the three coordinate axes in i-frame can be represented as

$$\dot{s}_1 = G_1(s_2)v_1 \tag{1}$$

where $G_1(s_2)$ is the translational velocity rotation matrix from the b-frame to the i-frame, which is given as

$$G_1(s_2) = \begin{bmatrix} a_{11} & a_{12} & a_{13} \\ a_{21} & a_{22} & a_{23} \\ a_{31} & a_{32} & a_{33} \end{bmatrix} \tag{2}$$

where $a_{11} = \cos\phi_y \cos\phi_z$, $a_{12} = \sin\phi_x \sin\phi_y \cos\phi_z - \cos\phi_x \sin\phi_z$, $a_{13} = \cos\phi_x \sin\phi_y \cos\phi_z + \sin\phi_x \sin\phi_z$, $a_{21} = \cos\phi_y \sin\phi_z$, $a_{22} = \sin\phi_x \sin\phi_y \sin\phi_z + \cos\phi_x \cos\phi_z$, $a_{23} = \cos\phi_x \sin\phi_y \sin\phi_z - \sin\phi_x \cos\phi_z$, $a_{31} = -\sin\phi_y$, $a_{32} = \sin\phi_x \cos\phi_y$, $a_{33} = \cos\phi_x \cos\phi_y$.

In addition, the angular velocity vector $\dot{s}_2$ around the three coordinate axes in i-frame can be described as

$$\dot{s}_2 = G_2(s_2)v_2 \tag{3}$$

where $G_2(s_2)$ is the rotational velocity rotation matrix from b-frame to the i-frame, which is defined as follows:

$$G_2(s_2) = \begin{bmatrix} 1 & \sin\phi_x \tan\phi_y & \cos\phi_x \tan\phi_y \\ 0 & \cos\phi_x & -\sin\phi_x \\ 0 & \sin\phi_x \sec\phi_y & \cos\phi_x \sec\phi_y \end{bmatrix}. \tag{4}$$

Finally, according to Eqs. (1)–(4), the kinematic equations of the AUV in 3-D space can be formulated as the following compact form:

$$\dot{s} = Gv \tag{5}$$

with

$$G = \begin{bmatrix} G_1(s_2) & O_{3*3} \\ O_{3*3} & G_2(s_2) \end{bmatrix} \tag{6}$$

$$s = [s_1, s_2]^T \tag{7}$$

$$v = [v_1, v_2]^T \tag{8}$$

where O_{3*3} is a 3×3 zero matrix.

2.3. Dynamic model

Dynamics mainly studies the relationship between the force acting on an AUV and the AUV motion. The dynamic equations of a 6-DOF AUV can be presented based on the Newton–Euler method as follows (Fossen, 2011):

$$M\dot{v} + C(v)v + D(v)v + g(s) = \tau \tag{9}$$

where $\tau = [F_{v_x}, F_{v_y}, F_{v_z}, F_{\omega_x}, F_{\omega_y}, F_{\omega_z}]^T$ represents the generalized external thrust forces and moments.

$M = (M_{RB} + M_A)$ denotes the inertia matrix. $M_{RB} = diag(m, m, m, I_x, I_y, I_z)$, is the rigid body mass matrix. $M_A = diag(-X_{\dot{v}_x}, -Y_{\dot{v}_y}, -Z_{\dot{v}_z}, -K_{\dot{\omega}_x}, -M_{\dot{\omega}_y}, -N_{\dot{\omega}_z})$ is the added inertia matrix.

$C(v)$ accounts for the Coriolis and centripetal matrix, which is expressed as

$$C(v) = C_{RB}(v) + C_A(V) \tag{10}$$

where

$$C_{RB}(v) = \begin{bmatrix} 0 & 0 & 0 & 0 & mv_z & -mv_y \\ 0 & 0 & 0 & -mv_z & 0 & mv_x \\ 0 & 0 & 0 & mv_y & -mv_x & 0 \\ 0 & mv_z & -mv_y & 0 & I_z\omega_z & -I_y\omega_y \\ -mv_z & 0 & mv_x & -I_z\omega_z & 0 & I_x\omega_x \\ mv_y & -mv_x & 0 & I_y\omega_y & -I_x\omega_x & 0 \end{bmatrix} \tag{11}$$

and

$$C_A(V)$$

$$= \begin{bmatrix} 0 & 0 & 0 & 0 & -Z_{\dot{v}_z}v_z & Y_{\dot{v}_y}v_y \\ 0 & 0 & 0 & Z_{\dot{v}_z}v_z & 0 & -X_{\dot{v}_x}v_x \\ 0 & 0 & 0 & -Y_{\dot{v}_y}v_y & X_{\dot{v}_x}v_x & 0 \\ 0 & -Z_{\dot{v}_z}v_z & Y_{\dot{v}_y}v_y & 0 & -N_{\dot{\omega}_z}\omega_z & M_{\dot{\omega}_y}\omega_y \\ Z_{\dot{v}_z}v_z & 0 & -X_{\dot{v}_x}v_x & N_{\dot{\omega}_z}\omega_z & 0 & -K_{\dot{\omega}_x}\omega_x \\ -Y_{\dot{v}_y}v_y & X_{\dot{v}_x}v_x & 0 & -M_{\dot{\omega}_y}\omega_y & K_{\dot{\omega}_x}\omega_x & 0 \end{bmatrix}. \tag{12}$$

$D(v) = diag(X_{v_x} + X_{|v_x|v_x}|v_x|, Y_{v_y} + Y_{|v_y|v_y}|v_y|, Z_{v_z} + Z_{|v_z|v_z}|v_z|, K_{\omega_x} + K_{|\omega_x|\omega_x}|\omega_x|, M_{\omega_y} + M_{|\omega_y|\omega_y}|\omega_y|, N_{\omega_z} + N_{|\omega_z|\omega_z}|\omega_z|)$ is the hydrodynamic damping matrix including the linear and quadratic drag.

$g(s)$ represents the vector of restoring forces and moments due to gravity and buoyancy, which is defined as

$$g(s) = \begin{bmatrix} (W - B)\sin\phi_y \\ -(W - B)\cos\phi_y \sin\phi_x \\ -(W - B)\cos\phi_y \cos\phi_x \\ y_B B\cos\phi_y \cos\phi_x - z_B B\cos\phi_y \sin\phi_x \\ -z_B B\sin\phi_y - x_B B\cos\phi_y \cos\phi_x \\ x_B B\cos\phi_y \sin\phi_x + y_B B\sin\phi_y \end{bmatrix}. \tag{13}$$

The symbols used in the above equations are defined as follows: m is the mass of the AUV; I_x, I_y and I_z are inertial tensors; $W = mg$ is the gravity and $B = bg$ is the buoyancy; x_B, y_B and z_B are the coordinates of the center of the AUV buoyancy in the b-frame. $X_{\dot{v}_x}$, $Y_{\dot{v}_y}$, $Z_{\dot{v}_z}$, $K_{\dot{\omega}_x}$, $M_{\dot{\omega}_y}$, $N_{\dot{\omega}_z}$, X_{v_x}, Y_{v_y}, Z_{v_z}, K_{ω_x}, M_{ω_y}, N_{ω_z}, $X_{|v_x|v_x}$, $Y_{|v_y|v_y}$, $Z_{|v_z|v_z}$, $K_{|\omega_x|\omega_x}$, $M_{|\omega_y|\omega_y}$, $N_{|\omega_z|\omega_z}$ are the hydrodynamic coefficients which can be directly or indirectly obtained in advance by practical experiments.

3. MPC-based trajectory tracking strategy

MPC is a numerical optimization-based control strategy, in which a system model is designed to predict the future control inputs and the future plant responses. It has a sound theoretical basis. By computing a sequence of future system input adjustment, the MPC controller attempts to optimize future plant responses at each regular interval (Qin and Badgwell, 2003). A system cost function is constructed which refers to the errors between the predicted system responses and the desired system outputs. By minimizing the cost function, the optimal control input sequence of the future N sampling instants can be obtained. During solving the optimization problem, the input and state constraints can be explicitly tackled, which can improve the robustness of the system. Rolling optimization and feedback correction are the main characteristics of MPC, which can effectively reduce or even eliminate the time-delay in a closed-loop system (Wang et al., 2018). Therefore, the MPC-based system can achieve excellent stability, optimality, and robustness (Mayne et al., 2000; Rawlings, 2002).

In this paper, the desired 3-D trajectory is assumed to be known in advance. A time parameterized triplet is introduced to determine the absolute position of the trajectory in the i-frame. The desired trajectory can be described in the following form:

$$Y_d(t) = [x_d(t)\ y_d(t)\ z_d(t)]^T. \tag{14}$$

We also assume that the desired trajectory is smooth and bounded, and appropriate by taking into account the physical limits of the AUV.

3.1. Prediction

In order to control the AUV motion, the kinematic model (5) is redefined in terms of the linear time-invariant (LTI) state–space representation with a sampling period T as follows:

$$s(k + 1) = s(k) + G(k)v(k)T \tag{15}$$

where $s(k)$, $G(k)$ and $v(k)$ are the system state vector, the rotation matrix and the control input vector at the kth sampling instant, respectively, with

$$s(k) = [x(k)\ y(k)\ z(k)\ \phi_x(k)\ \phi_y(k)\ \phi_z(k)]^T \tag{16}$$

$$v(k) = [v_x(k)\ v_y(k)\ v_z(k)\ \omega_x(k)\ \omega_y(k)\ \omega_z(k)]^T. \tag{17}$$

However, the velocity of the AUV cannot be changed sharply in the actual underwater environment due to physical limits. Therefore, the optimal control inputs obtained by the model predictive control method may not be accepted and executed by the AUV. To solve this problem, an incremental version of (15) is introduced with the control input vector

$$u(k) = v(k) - v(k - 1). \tag{18}$$

The improved model with state–space representation can be expressed as

$$X(k + 1) = A(k)X(k) + B(k)u(k) \tag{19}$$

$$Y(k) = CX(k) \tag{20}$$

with

$$X(k) = [s(k)\ v(k - 1)]^T \tag{21}$$

$$A(k) = \begin{bmatrix} I_6 & G(k)T \\ O_{6*6} & I_6 \end{bmatrix} \tag{22}$$

$$B(k) = \begin{bmatrix} G(k)T \\ I_6 \end{bmatrix} \tag{23}$$

$$Y(k) = s(k) \tag{24}$$

$$C = [I_3\ O_{3*9}] \tag{25}$$

where I_6, O_{6*6}, and O_{3*6} denote a 6×6 identity matrix, a 6×6 zero matrix, and a 3×6 zero matrix, respectively.

Remark 1. The state $X(k + 1)$ is derived as follows:

$$X(k + 1) = \begin{bmatrix} s(k + 1) \\ v(k) \end{bmatrix} = \begin{bmatrix} s(k) + G(k)v(k)T \\ v(k) \end{bmatrix}$$

$$= \begin{bmatrix} s(k)+G(k)v(k)T + G(k)v(k-1)T - G(k)v(k-1)T \\ v(k) + v(k-1) - v(k-1) \end{bmatrix}$$

$$= \begin{bmatrix} s(k)+ G(k)v(k-1)T \\ v(k-1) \end{bmatrix} + \begin{bmatrix} G(k)v(k)T - G(k)v(k-1)T \\ v(k) - v(k-1) \end{bmatrix}$$

$$= \begin{bmatrix} I_6 & G(k)T \\ O_{6*6} & I_6 \end{bmatrix}\begin{bmatrix} s(k) \\ v(k-1) \end{bmatrix} + \begin{bmatrix} G(k)T \\ I_6 \end{bmatrix}[\ v(k)-v(k-1)\ ]$$

$$= A(k)X(k) + B(k)u(k).$$

According to the state prediction model (19), given an input sequence, the corresponding prediction state sequence of the system can be calculated by simulating the model forward over N sampling

intervals, where N is termed as prediction horizon. For notational convenience, the input sequence and predicted state sequence are often stacked into vectors $U(k)$ and $\overline{X}(k)$, respectively. $U(k)$ and $\overline{X}(k)$ are described as

$$U(k) = \begin{bmatrix} u(k|k) \\ u(k+1|k) \\ \vdots \\ u(k+N-1|k) \end{bmatrix}, \overline{X}(k) = \begin{bmatrix} X(k+1|k) \\ X(k+2|k) \\ \vdots \\ X(k+N|k) \end{bmatrix} \tag{26}$$

where $u(k + i|k)$ and $X(k + i|k)$ are the input vector and state vector at time $k + i$ predicted at time k, respectively.

To make the AUV move more steadily, the rotation along three axes should be decreased during the practical trajectory tracking task. For this reason, in order to reduce the computational effort, we assume that the velocity rotation matrix $G(k)$, coefficient matrix $A(k)$ and $B(k)$ are invariant during the prediction stage. Then, $X(k+i|k)$ can be calculated according to (19) by

$$X(k+i|k) = A(k)X(k+i-1|k) + B(k)u(k+i-1|k) \tag{27}$$

$$= A(k)^i X(k|k) + \sum_{j=0}^{i-1} A(k)^{i-1-j} B(k)u(k + j) \tag{28}$$

with the initial condition $X(k|k) = X(k)$.

Based on Eqs. (27) and (28), the $\overline{X}(k)$ can be re-expressed as

$$\overline{X}(k) = \overline{A}(k)x(k) + \overline{B}(k)U(k) \tag{29}$$

where

$$\overline{A}(k) = [A(k)\ A(k)^2\ \cdots\ A(k)^N]^T \tag{30}$$

and

$$\overline{B}(k) = \begin{bmatrix} B(k) & 0 & \cdots & 0 \\ A(k)B(k) & B(k) & \cdots & 0 \\ \vdots & \vdots & \ddots & \vdots \\ A(k)^{N-1}B(k) & A(k)^{N-2}B(k) & \cdots & B(k) \end{bmatrix}. \tag{31}$$

3.2. Constraints handling

In an actual trajectory tracking task, the AUV faces several constraints. These constraints can be either soft constraints or hard constraints. If necessary, soft constraints may be violated to avoid infeasibility. But hard constraints must always be satisfied. In the trajectory tracking task, the system state vector $x(k)$ has a lower bound and an upper bound, and the range of input vector $u(k)$ also has constraints. Thus, the following constraints should be imposed on the system.

$$u_{min} \leq u(k) \leq u_{max} \tag{32}$$

$$X_{min} \leq X(k) \leq X_{max} \tag{33}$$

where u_{min}, X_{min} are the predefined lower bounds, and u_{max}, X_{max} are the predefined upper bounds.

By translating the constraints for state $X(k)$ into constraints for input $u(k)$, and stacking everything into a compact matrix form, the input and state constraints can be rewritten as

$$U(k) \leq U_{max} \tag{34}$$

$$-U(k) \leq -U_{min} \tag{35}$$

$$\overline{A}(k)X(k) + \overline{B}(k)U(k) \leq \overline{X}_{max} \tag{36}$$

$$-\overline{A}(k)X(k) - \overline{B}(k)U(k) \leq -\overline{X}_{min}. \tag{37}$$

Constraints (34)–(37) can be expressed in the following compact linear constraint form:

$$LU(k) \leq l \tag{38}$$

where

$$L = \begin{bmatrix} I_{6N} \\ -I_{6N} \\ \overline{B}(k) \\ -\overline{B}(k) \end{bmatrix}, \quad l = \begin{bmatrix} U_{max} \\ -U_{min} \\ \overline{X}_{max} - \overline{A}(k)X(k) \\ -\overline{X}_{min} + \overline{A}(k)X(k) \end{bmatrix}. \tag{39}$$

3.3. Optimization

In this section, a controller is designed so that the AUV can be steered to a desired trajectory stably and precisely. The optimization problem is solved regularly to minimize a predicted performance cost (denoted by J) by adjusting the current and future inputs of the system. The predicted performance cost is defined as follows:

$$J = \int_0^T [\|Y(t) - Y_d(t)\|_{Q_y}^2 + \|u(t)\|_{Q_u}^2] \, dt \tag{40}$$

where $\|x\|_Q^2 = x^T Q x$; $Y(t)$ and $Y_d(t)$ are the predicted trajectory and the desired trajectory, respectively; $u(t)$ denotes the predicted inputs; Q_y and Q_u are the symmetric positive definite weight matrices.

We can see that the performance cost J includes an integral operation. To address the optimization problem, the integral operation need to be performed numerically in practice. Here, we divide T into N steps, and the discretized version of $J(k)$ at the sampling instant k can be represented as

$$J(k) = \sum_{i=1}^{N} [\|Y(k+i|k) - Y_d(k+i)\|_{Q_y}^2 + \|u(k+i-1|k)\|_{Q_u}^2] \tag{41}$$

where $Y(k+i|k)$ and $u(k+i-1|k)$ denote the predicted position and system input at time $k+i$ predicted at time k; $Y_d(k+i)$ is the desired position at time $k+i$.

For a given $Y(k)$, $X(k)$ can be calculated by

$$X(k) = C^+ Y(k) \tag{42}$$

where C^+ denotes the pseudoinverse of matrix C.

By substituting (42) into (41), we can obtain another discretized version of $J(k)$ represented by

$$J(k) = \sum_{i=1}^{N} [\|X(k+i|k) - X_d(k+i)\|_{Q_x}^2 + \|u(k+i-1|k)\|_{Q_u}^2] \tag{43}$$

where

$$X_d(k+i) = C^+ Y_d(k+i) \tag{44}$$

$$Q_x = C^+ Q_y C. \tag{45}$$

According to (29), a simplified version of $J(k)$ can be represented by

$$J(k) = \|\overline{X}(k) - \overline{X_d}(k)\|_{\overline{Q}_x}^2 + \|U(k)\|_{\overline{Q}_u}^2$$

$$= \|\overline{A}(k)x(k) + \overline{B}(k)U(k) - \overline{X_d}(k)\|_{\overline{Q}_x}^2 + \|U(k)\|_{\overline{Q}_u}^2. \tag{46}$$

where

$$\overline{X_d}(k) = \begin{bmatrix} X_d(k+1) \\ X_d(k+2) \\ \vdots \\ X_d(k+N) \end{bmatrix} \tag{47}$$

$$\overline{Q}_x = \begin{bmatrix} Q_x & 0 & \cdots & 0 \\ 0 & Q_x & \cdots & 0 \\ \vdots & \vdots & \ddots & \vdots \\ 0 & 0 & \cdots & Q_s \end{bmatrix} \tag{48}$$

$$\overline{Q}_u = \begin{bmatrix} Q_u & 0 & \cdots & 0 \\ 0 & Q_u & \cdots & 0 \\ \vdots & \vdots & \ddots & \vdots \\ 0 & 0 & \cdots & Q_u \end{bmatrix}. \tag{49}$$

From (46), it can be noticed that $J(k)$ is a function of $U(k)$. Then, the optimization problem can be expressed as follows:

$$U^*(k) = \arg\min_{U(k)} J(k)$$

$$s.t. \quad LU(k) \le l \tag{50}$$

where $U^*(k)$ denotes the optimal input sequence.

The constrained optimization problem (50) is rather complicated to calculate. Fortunately, it can be transformed into a convex quadratic programming (QP) problem which a QP solver can be utilized to solve online over a finite receding horizon. It has been proved that the standard convex QP optimization problem has a unique optimal solution (Boyd and Vandenberghe, 2004), which shows the stability of our method. After a series of deductions, the final standard convex QP form of (50) can be represented as follows:

$$U^*(k) = \arg\min_{U(k)} \frac{1}{2} U^T(k) H(k) U(k) + f^T(k) U(k)$$

$$s.t. \quad LU(k) \le l \tag{51}$$

with

$$H(k) = 2(\overline{B}^T(k)\overline{Q}_x\overline{B}(k) + \overline{Q}_u)$$

$$f(k) = 2\overline{B}^T(k)\overline{Q}_x(\overline{A}(k)x(k) - \overline{X}_d(k)).$$

3.4. Receding horizon implementation

The QP problem (51), involving linear input and state constraints (38), can be computed online. Then an predicted optimal input vector $U^*(k)$ is obtained. however, only the first element of $U^*(k)$ is used by the AUV.

$$u(k) = u^*(k|k) \tag{52}$$

According to (18), the derivative of $v(k)$ by time can be obtained as:

$$\dot{v}(k) = u(k)/T \tag{53}$$

Once $\dot{v}(k)$ has been determined, the approximate forces and moments vector $\tau(k)$ which are needed to achieve the desired accelerations can be estimated by the dynamic inversion.

$$\tau(k) = M\dot{v}(k) + C(v(k-1))v(k-1) + D(v(k-1))v(k-1) + g(s(k-1)) \tag{54}$$

Based on the dynamic Eqs. (9)–(13), the independent system control at the kth sampling instant can be expressed as follows:

$$F_{v_x}(k) = (m - X_{\dot{v}_x}) \dot{v}_x + n_1(s(k-1), v(k-1)) \tag{55}$$

$$F_{v_y}(k) = (m - Y_{\dot{v}_y}) \dot{v}_y + n_2(s(k-1), v(k-1)) \tag{56}$$

$$F_{v_z}(k) = (m - Z_{\dot{v}_z}) \dot{v}_z + n_3(s(k-1), v(k-1)) \tag{57}$$

$$F_{\omega_x}(k) = (I_x - K_{\dot{\omega}_x})\dot{\omega}_x + n_4(s(k-1), v(k-1)) \tag{58}$$

$$F_{\omega_y}(k) = (I_y - M_{\dot{\omega}_y})\dot{\omega}_x + n_5(s(k-1), v(k-1)) \tag{59}$$

$$F_{\omega_z}(k) = (I_z - N_{\dot{\omega}_z}) \dot{\omega}_x + n_6(s(k-1), v(k-1)) \tag{60}$$

where

$$N(s(k-1), v(k-1)) \triangleq C(v(k-1))v(k-1) + D(v(k-1))v(k-1) + g(s(k-1))$$

$$= [n_i(s(k-1), v(k-1))], i \in \{1, 2, 3, 4, 5, 6\}. \tag{61}$$

At each sampling instant k, the $U^*(k)$ is recalculated. Then, the optimal control forces $F_{v_x}, F_{v_y}, F_{v_z}$ and control moments $F_{\omega_x}, F_{\omega_y}, F_{\omega_z}$ are computed and executed by the AUV repeatedly to achieve the rolling optimization. The predicted state vector $\overline{X}(k)$ and the optimal input vector $U^*(k)$ are only determined by the current state $X(k)$. Therefore, the MPC method can provide a degree of robustness to modeling errors and time-varying disturbances in complex ocean. The optimization process iterates until the AUV finish the trajectory tracking task.

3.5. Algorithm

The complete MPC-based trajectory tracking control algorithm is summarized in Algorithm 1.

Algorithm 1 MPC-based 3-D Trajectory Tracking Algorithm

Input: $X(0)$ (initial state), Y_d (desired trajectory), N (prediction horizon), C (coefficient matrix), Q_u, Q_y (weighting matrices), u_{min}, u_{max} (input constraints), X_{min}, X_{max} (state constraints)

1: $k \leftarrow 1$
2: $X(k) \leftarrow X(0)$
3: Compute Q_x, $\overline{Q}_x$, $\overline{Q}_u$, U_{min}, U_{max}, $\overline{X}_{min}$, and $\overline{X}_{max}$
4: **while** $k \le len(Y_d)$ **do**
5:      Update $G(k)$, $A(k)$, and $B(k)$ using (6), (22), (23)
6:      Compute $\overline{A}(k)$, $\overline{B}(k)$, L, and l using (30), (31), (39)
7:      Solve the QP problem (51)
8:      Get the first control input $u(k)$ from $U^*(k)$
9:      Compute the forces and moments vector $\tau(k)$ using (55)-(61)
10:      Implement $\tau(k)$ to the AUV
11:      $k \leftarrow k + 1$
12:      Measure the current state $X(k)$
13: **end while**

---

4. Simulation results

In this section, simulations are performed to verify the feasibility and robustness of the proposed MPC-based method. All simulations are done on a laptop with an Intel Core i5-4220U 2.30-GHz dual-core processor using a simulator developed on Matlab R2017a platform. Two types of desired trajectories are chosen. The first is a raster scan trajectory, and the second is a sinusoidal trajectory.

Each simulation is performed with or without ocean disturbances. Let dx, dy, and dz be the disturbances with respect to X_G-axis, Y_G-axis, and Z_G-axis in the i-frame, respectively. There are three kinds of disturbances considered in the following simulations. The first is a *random disturbance* defined as

$$\begin{cases} dx = 0.4 * randn(1) \text{ m/s} \\ dy = 0.3 * randn(1) \text{ m/s} \\ dz = 0.2 * randn(1) \text{ m/s} \end{cases} \quad (62)$$

the second is an *ocean current disturbance* defined as

$$\begin{cases} dx = -0.2 \text{ m/s} \\ dy = 0.2 \text{ m/s} \\ dz = 0.2 \text{ m/s,} \end{cases} \quad (63)$$

and the third is an *ocean wave disturbance* defined as

$$\begin{cases} dx = -0.35 \cos(t\pi/8) \text{ m/s} \\ dy = 0.35 \cos(t\pi/8) \text{ m/s} \\ dz = 0.3 \cos(t\pi/8) \text{ m/s} \end{cases} \quad (64)$$

where randn(1) is a normal distribution noise signal with 0 mean and 1 variance.

In all simulations, the values of the parameters with respect to the AUV dynamics are obtained from the identified dynamic model of Falcon (Proctor, 2014) and are shown in Table 1. The values of the parameters with respect to the MPC algorithm are as follows: the sampling period $T = 0.5$ s, the prediction horizon $N = 10$, the weighting matrices $Q_y = diag(1, 1, 1, 1, 1, 1, 1)$, $Q_u = diag(0.1, 0.1, 0.1, 0.1, 0.1, 0.1)$, the initial state vector $s(0) = [0, 6, -52, 0, 0, 0]^T$, the initial velocity vector $v(0) = [0, 0, 0, 0, 0, 0]^T$, the input constraints $u_{max} = [0.2, 0.2, 0.2, 0.05, 0.05, 0.05]^T$ and $u_{min} = [-0.2, -0.2, -0.2, -0.05, -0.05, -0.05]^T$, the state constraints $X_{max} = [+\infty, +\infty, 0, \pi, 2\pi/5, \pi, 2, 2, 2, \pi/18, \pi/18, \pi/18]^T$, $X_{min} = [-\infty, -\infty, -\infty, -\pi, -2\pi/5, -\pi, -2, -2, -2, -\pi/18, -\pi/18, -\pi/18]^T$.

Table 1
Values of the AUV inertia and hydrodynamic parameters.

Parameters	Value	Parameters	Value
m	116 kg	b	116.2 kg
$X_{\dot{v}_x}$	-167.6 kg	I_x	9.3 kgm^2
$Y_{\dot{v}_y}$	-477.2 kg	I_y	14.9 kgm^2
$Z_{\dot{v}_z}$	-235.7 kg	I_z	13.1 kgm^2
$K_{\dot{\omega}_x}$	-11.6 kgm^2	x_B	-0.00045 m
$M_{\dot{\omega}_y}$	-15.5 kgm^2	y_B	-0.00128 m
$N_{\dot{\omega}_z}$	-15.9 kgm^2	z_B	-0.04298 m
X_{v_x}	26.9 kg/s	$X_{|v_x|v_x}$	241.3 kg/m
Y_{v_y}	35.8 kg/s	$Y_{|v_y|v_y}$	503.8 kg/m
Z_{v_z}	6.19 kg/s	$Z_{|v_z|v_z}$	119.1 kg/m
K_{ω_x}	3.0 kgm^2/(s · rad)	$K_{|\omega_x|\omega_x}$	101.6 kgm^2/rad^2
M_{ω_y}	4.9 kgm^2/(s · rad)	$M_{|\omega_y|\omega_y}$	59.9 kgm^2/rad^2
N_{ω_z}	3.5 kgm^2/(s · rad)	$N_{|\omega_z|\omega_z}$	76.9 kgm^2/rad^2
g	9.8 N/kg		

4.1. Tracking of raster scan trajectory

A common trajectory tracking task for an AUV equipped with survey instruments to execute is raster scan. A raster scan makes the AUV to cover an area of interest. The raster scan reference trajectory is defined as follows:

$$Y_d(t) = \begin{cases} [t, 0, 3t/22 - 50]^T \text{ m,} & 0 \text{ s} \le t < 60 \text{ s} \\ [60, t - 60, 3t/22 - 50]^T \text{ m,} & 60 \text{ s} \le t < 80 \text{ s} \\ [140 - t, 20, 3t/22 - 50]^T \text{ m,} & 80 \text{ s} \le t < 140 \text{ s} \\ [0, t - 120, 3t/22 - 50]^T \text{ m,} & 140 \text{ s} \le t < 160 \text{ s} \\ [t - 160, 40, 3t/22 - 50]^T \text{ m,} & 160 \text{ s} \le t < 220 \text{ s} \end{cases} \quad (65)$$

In the raster scan task, the AUV encounters several straight lines and sharp turns. To verify the performance of our algorithm, the initial location of the AUV is chosen as $[0, 6, -52]^T$ m in the i-frame, which is not the same with the starting location of the desired trajectory.

Fig. 2 shows the trajectory tracking results of the raster scan task in 3-D space. The red curve is the simulated tracking result without disturbance, the blue curve represents the simulated tracking result with random disturbance, the green curve represents the simulated tracking result under ocean current, and the pink curve represents the simulated tracking results under ocean wave, while the black curve represents the desired raster scan trajectory. As can be seen that the AUV can successfully achieve the realtime tracking of the desired raster scan trajectory with or without disturbances.

The curves of position tracking performances in three directions versus time are plotted in Fig. 3. It can be readily observed that (i) in all simulations, the AUV is successfully steered to closely track the desired trajectory despite the presence of initial errors; (ii) the MPC-based method can achieve excellent performance in the absence of disturbances; (iii) when the AUV deviates from the trajectory due to disturbances, the MPC-based method can make the AUV approach the desired trajectory quickly.

The main performance metric used in this paper is position tracking error, which refers to the distance between the actual position and the desired position in 3-D space. The position tracking error at the kth sampling instant is defined as follows:

$$e(k) = \sqrt{(x(k) - x_d(k))^2 + (y(k) - y_d(k))^2 + (z(k) - z_d(k))^2} \quad (66)$$

where $x(k), y(k), z(k)$ are the actual position and $x_d(k), y_d(k), z_d(k)$ are the desired position.

The position tracking error is a true measurement of the difference between the actual trajectory and the desired trajectory. The curves of position tracking error versus time are shown in Fig. 4.

Since the initial position of AUV is different from the starting point of the desired trajectory, the position tracking errors are large in the beginning. After about 10 s, the errors go to around 0. From Fig. 4, it can be shown that the position tracking errors suddenly increase
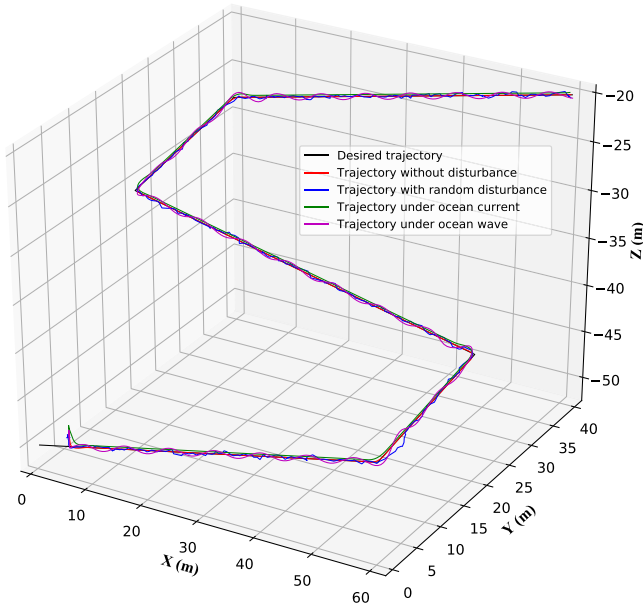
Fig. 2. AUV 3-D trajectories for raster scan task under different disturbances. (For interpretation of the references to color in this figure legend, the reader is referred to the web version of this article.)
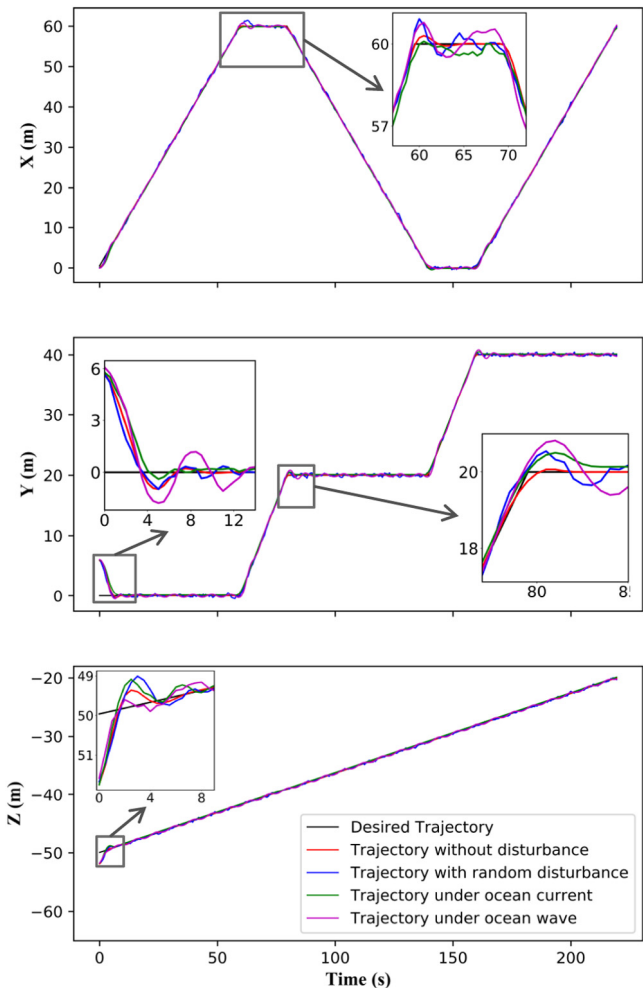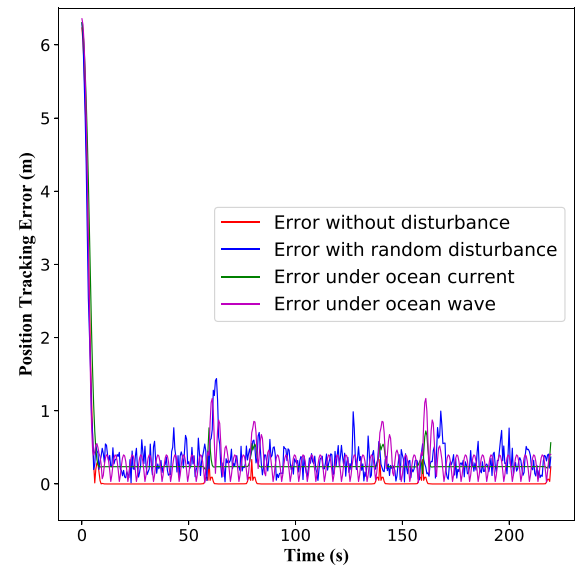

Fig. 4. Position tracking errors for raster scan task under different disturbances.

Table 2
Position tracking error measurements after 5 s for raster scan task.

Disturbances	Maximum(m)	Minimum(m)	Average(m)
None	0.6613	0.0000	0.0137
Random	1.4399	0.0172	0.3235
Ocean current	1.5343	0.1425	0.2597
Ocean wave	1.1683	0.0183	0.3087

at 60 s, 80 s, 140 s and 160 s. This is because the AUV encounters sharp turns of 90 degrees. Another observation can be made is that the position tracking errors with disturbances are larger than those without disturbance. This is because these disturbances cause the AUV to deviate from the desired trajectory. For the sake of clarity, the position tracking error measurements after 5 s are listed in Table 2. It can be seen that the average of position tracking errors without disturbance is very small (about 0.0137 m) for an AUV with a speed of more than 1 m/s. Moreover, the average of position tracking errors with disturbances is about 0.3 m, which demonstrates the good performance of our method.

Fig. 5 shows the curves of actual control forces and moments versus time under different disturbances. The actual control forces and moments without disturbance are stable and change very slowly (red curves). However, the actual control forces and moments with disturbances change significantly. This is because the position of the AUV deviates from the desired trajectory due to disturbances, and the AUV needs to change the control forces and moments dramatically to approach the desired trajectory as early as possible.

4.2. Tracking of sinusoidal trajectory

Another task for an AUV to execute is tracking a curve trajectory, which is rather different from the raster scan trajectory. The sinusoidal reference trajectory is a curve trajectory defined as follows:

$$Y_d(t) = \begin{bmatrix} t \text{ m} \\ 25\sin(0.1t) \text{ m} \\ 3t/10 - 50 \text{ m} \end{bmatrix}, \quad 0\text{ s} \le t < 100\text{ s} \tag{67}$$

In the sinusoidal trajectory tracking task, the AUV encounters several curves with different degrees of curvature. The sinusoidal trajectory tracking results in 3-D space are shown in Fig. 6.

The position tracking performances in three directions are plotted in Fig. 7, the position tracking errors are recorded in Fig. 8 and the
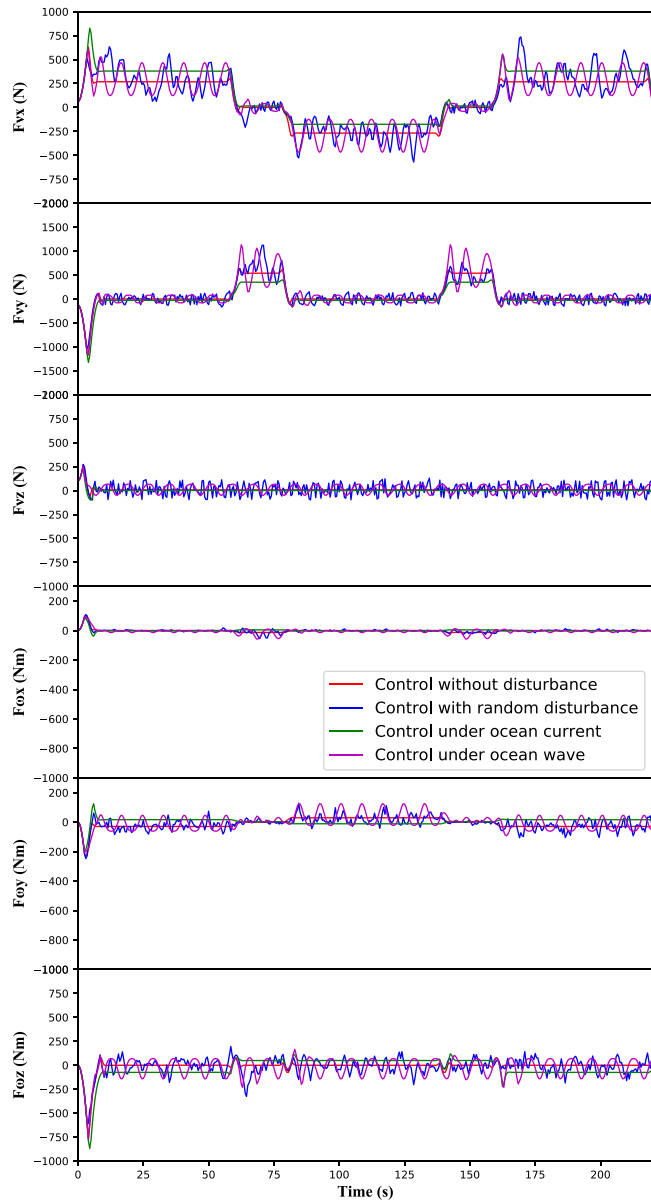

Fig. 3. Position tracking performances for raster scan task under different disturbances.

Fig. 5. Actual control forces and moments for raster scan task under different disturbances. (For interpretation of the references to color in this figure legend, the reader is referred to the web version of this article.)

Table 3
Position tracking error measurements after 5 s for sinusoidal tracking task.

Disturbances	Maximum(m)	Minimum(m)	Average(m)
None	0.3174	0.0000	0.0066
Random	1.0083	0.0557	0.3331
Ocean current	0.5782	0.2184	0.2414
Ocean wave	1.1629	0.0286	0.2804

position tracking error measurements after 5 s are listed in Table 3. Similar observations can be made that the AUV can be successfully steered to the desired sinusoidal trajectory in real time with or without disturbances.

As can be seen from both Figs. 7 and 8, the actual trajectory of the AUV without disturbance basically coincides with the desired trajectory (red curves). At the beginning of the simulations, the position tracking errors are large since the initial position is not the same as the starting point of the desired trajectory. But as time goes by, the position tracking
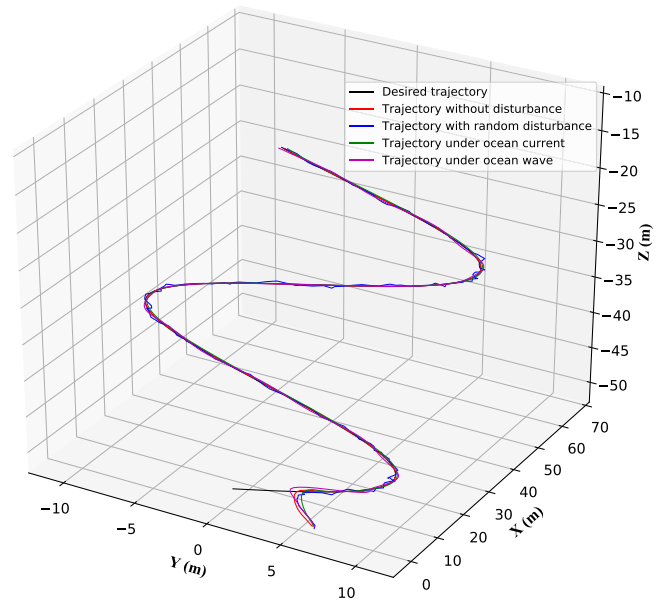

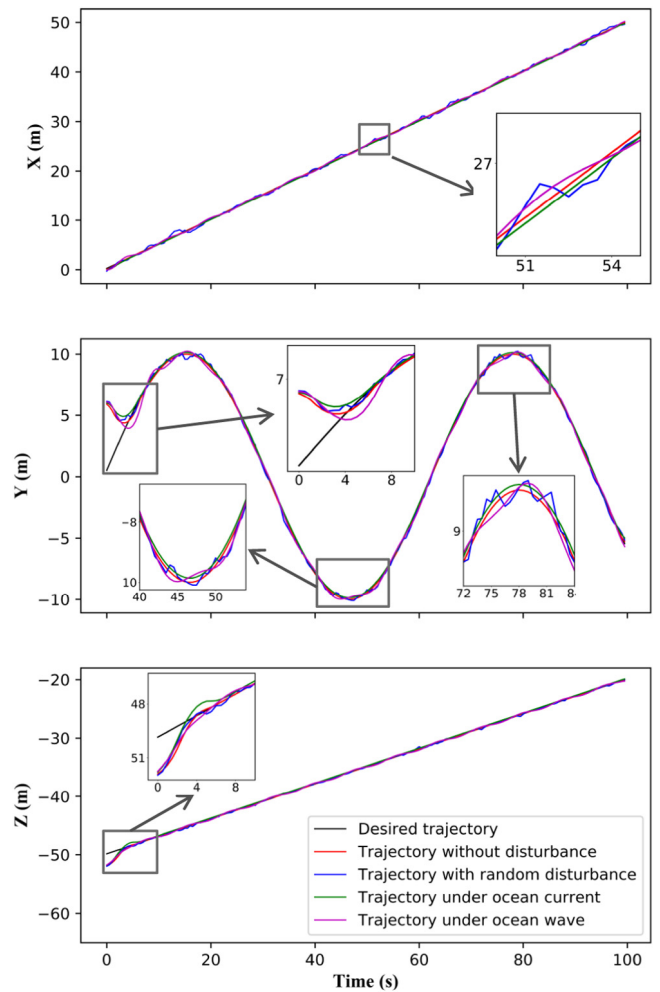**Fig. 6.** AUV 3-D trajectories for sinusoidal tracking task under different disturbances.

Fig. 7. Position tracking performances for sinusoidal tracking task under different disturbances. (For interpretation of the references to color in this figure legend, the reader is referred to the web version of this article.)
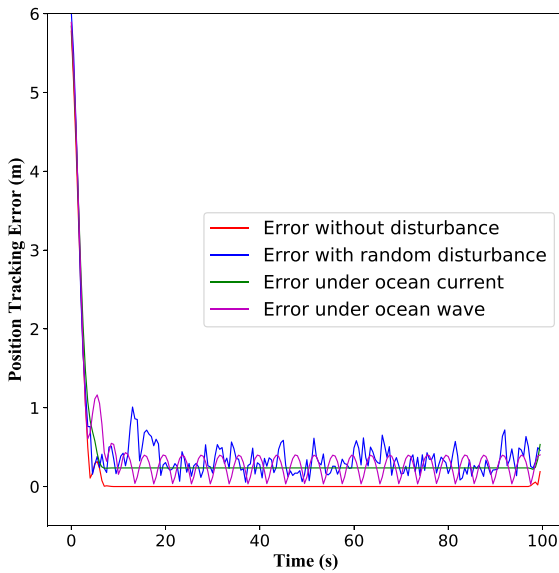
Fig. 8. Position tracking errors for sinusoidal tracking task under different disturbances. (For interpretation of the references to color in this figure legend, the reader is referred to the web version of this article.)

errors gradually decrease and tend to zero. Because there are no sharp changes of direction in the sinusoidal trajectory tracking, the position tracking errors are very small during the whole task (an average of 0.0066 m without disturbance).

The actual control forces and moments for sinusoidal tracking task under different disturbances are depicted in Fig. 9. The same as the raster scan trajectory tracking, the actual control forces and moments without disturbance are stable and change very slowly (red curves). The simulation results under various disturbances further illustrate the robustness of our MPC-based method.

5. Conclusion

In this paper, a novel MPC-based 3-D trajectory tracking strategy for AUVs has been presented. Firstly, the kinematic analysis of an fully-actuated AUV is conducted and the 6-DOF kinematics and dynamics equation are established. Secondly, the practical input and state constraints are considered explicitly. Meanwhile, for convenience, the state constraints are translated into the input constraints. Thirdly, the control increments are introduced as the system input to improve the stability of the AUV. Finally, the trajectory tracking problem is transformed into a constrained standard QP problem which can be computed online. During an actual trajectory tracking in the complex ocean environment, the AUV encounters various disturbances, such as random disturbances, ocean current disturbances and ocean wave disturbances. Because the optimal control inputs are recalculated at each sampling instant, the trajectory tracking task can be well accomplished even though the AUV are under these disturbances. Simulation studies of tracking two different types of reference trajectories have been conducted and have demonstrated the feasibility and robustness of the MPC-based algorithm under uncertain disturbances in the complex ocean environment.
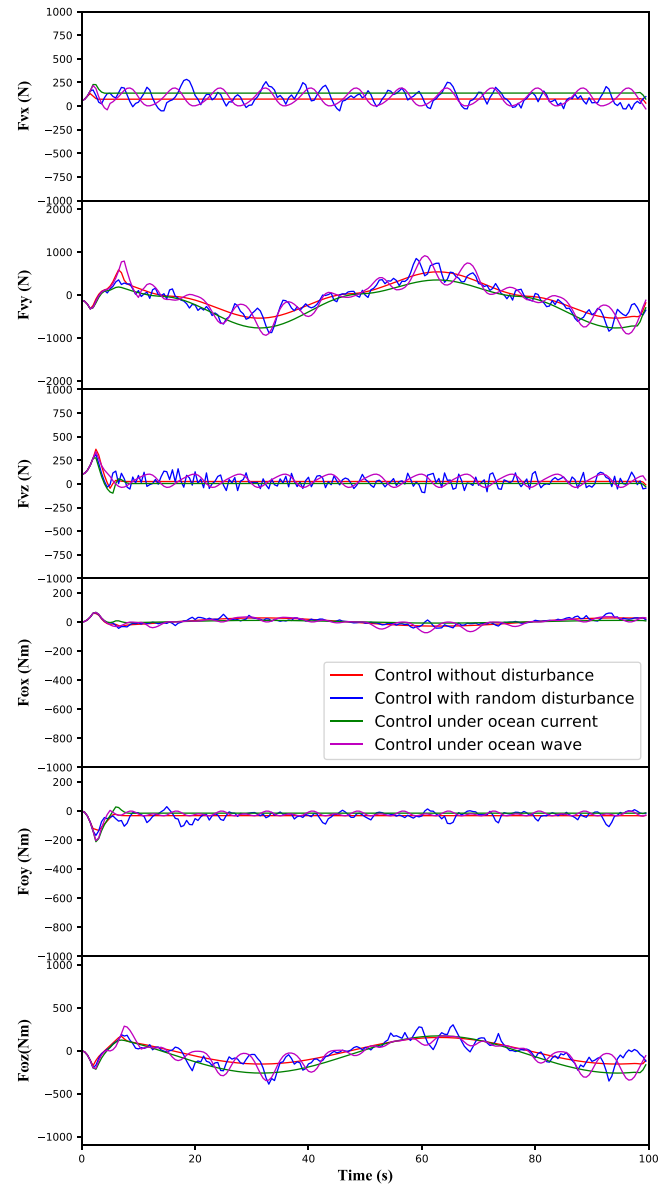
Fig. 9. Actual Control forces and moments for sinusoidal tracking task under different disturbances. (For interpretation of the references to color in this figure legend, the reader is referred to the web version of this article.)

References

Aguiar, A.P., Hespanha, J.P., 2007. Trajectory-tracking and path-following of under-actuated autonomous vehicles with parametric modeling uncertainty. IEEE Trans. Automat. Control 52 (8), 1362–1379.

Antonelli, G., Chiaverini, S., Sarkar, N., West, M., 2001. Adaptive control of an autonomous underwater vehicle: experimental results on ODIN. IEEE Trans. Syst. Man Cybern. 9 (5), 756–765.

Beal, C.E., Gerdes, J.C., 2013. Model predictive control for vehicle stabilization at the limits of handling. IEEE Trans. Control Syst. Technol. 21 (4), 1258–1269.

Boyd, S., Vandenberghe, L., 2004. Convex Optimization. Cambridge University Press, U.K..

Cui, R., Zhang, X., Cui, D., 2016. Adaptive sliding-mode attitude control for autonomous underwater vehicles with input nonlinearities. Ocean Eng. 123, 45–54.

Do, K.D., Pan, J., 2009. Control of Ships and Underwater Vehicles:design for Underactuated and Nonlinear Marine Systems. Springer-Verlag, London, U.K..

Ferri, G., Munaf, A., Lepage, K.D., 2018. An autonomous underwater vehicle data-driven control strategy for target tracking. IEEE J. Ocean. Eng. 43 (2), 323–343.

Fossen, T.I., 2011. Handbook of Marine Craft Hydrodynamics and Motion Control. John Wiley & Sons.

Gan, W., Zhu, D., Ji, D., 2018. QPSO-model predictive control-based approach to dynamic trajectory tracking control for unmanned underwater vehicles. Ocean Eng. 158, 208–220.

Gao, J., Liu, C., Proctor, A., 2016. Nonlinear model predictive dynamic positioning control of an underwater vehicle with an onboard USBL system. J. Mar. Sci. Technol. 21 (1), 57–69.

Hammad, M.M., Elshenawy, A.K., El Singaby, M.I., 2017. Trajectory following and stabilization control of fully actuated AUV using inverse kinematics and self-tuning fuzzy PID. PLoS One 12 (7), e0179611.

Jalving, B., 1994. The NDRE-AUV flight control system. IEEE J. Ocean. Eng. 19 (4), 497–501.

Ji, H., Pan, M., Wonhong, S., Sang, J., 2007. Stable nonlinear adaptive controller for an autonomous underwater vehicle using neural networks. Internat. J. Systems Sci. 38 (4), 327–337.

Khodayari, M.H., Balochian, S., 2015. Modeling and control of autonomous underwater vehicle (AUV) in heading and depth attitude via self-adaptive fuzzy PID controller. J. Mar. Sci. Technol. 20 (3), 559–578.

Kim, J., Joe, H., Yu, S.C., Jin, S.L., Kim, M., 2016. Time-delay controller design for position control of autonomous underwater vehicle under disturbances. IEEE Trans. Ind. Electron. 63 (2), 1052–1061.

Londhe, P.S., Dhadekar, D.D., Patre, B.M., Waghmare, L.M., 2017. Uncertainty and disturbance estimator based sliding mode control of an autonomous underwater vehicle. Int. J. Dyn. Control 5 (4), 1122–1138.

Mayne, D., Rawlings, J., Rao, C., Scokaert, P., 2000. Constrained model predictive control: Stability and optimality. Automatica 36 (6), 789–814.

Park, B.S., 2015. Neural network-based tracking control of underactuated autonomous underwater vehicles with model uncertainties. J. Dyn. Syst. Meas. Control 137 (2), 1–7.

Park, B.S., Yoo, S.J., Jin, B.P., Choi, Y.H., 2010. A simple adaptive control approach for Trajectory tracking of electrically driven nonholonomic mobile robots. IEEE Trans. Control Syst. Technol. 18 (5), 1199–1206.

Peng, Z., Wang, J., Han, Q., 2019a. Path-following control of autonomous underwater vehicles subject to velocity and input constraints via Neurodynamic optimization. IEEE Trans. Ind. Electron. 66 (11), 8724–8732.

Peng, Z., Wang, J., Wang, J., 2019b. Constrained control of autonomous underwater vehicles based on command optimization and disturbance estimation. IEEE Trans. Ind. Electron. 66 (5), 3627–3635.

Perrier, M., Canudas-De-Wit, C., 1996. Experimental comparison of PID vs. PID plus nonlinear controller for subsea robots. Auton. Robots 3 (2–3), 195–212.

Proctor, A.A., 2014. Semi-Autonomous Guidance and Control of a Saab Seaeye Falcon ROV (Ph.D. thesis). Department of Mechanical Engineering, University of Victoria, Victoria, BC, Canada.

Qiao, L., Yi, B., Wu, D., Zhang, W., 2017. Design of three exponentially convergent robust controllers for the trajectory tracking of autonomous underwater vehicles. Ocean Eng. 134, 157–172.

Qiao, L., Zhang, W., 2019a. Adaptive second-order fast nonsingular terminal sliding mode tracking control for fully actuated autonomous underwater vehicles. IEEE J. Ocean. Eng. 44 (2), 363–385.

Qiao, L., Zhang, W., 2019b. Double-loop integral terminal sliding mode tracking control for UUVs with adaptive dynamic compensation of uncertainties and disturbances. IEEE J. Ocean. Eng. 44 (1), 29–53.

Qin, S.J., Badgwell, T.A., 2003. A survey of industrial model predictive control technology. Control Eng. Pract. 11 (7), 733–764.

Rawlings, J.B., 2002. Tutorial overview of model predictive control. IEEE Control Syst. Mag. 20 (3), 38–52.

Refsnes, J.E., Sorensen, A.J., Pettersen, K.Y., 2008. Model-based output feedback control of slender-body underactuated AUVs: theory and experiments. IEEE Trans. Control Syst. Technol. 16 (5), 930–946.

Sahu, B.K., Subudhi, B., 2014. Adaptive tracking control of an autonomous underwater vehicle. Int. J. Auto. Comput. 11 (3), 299–307.

Shen, C., Buckham, B., Shi, Y., 2017. Modified C/GMRES algorithm for fast nonlinear model predictive tracking control of AUVs. IEEE Trans. Control Syst. Technol. 25 (5), 1896–1904.

Shen, C., Shi, Y., Buckham, B., 2018. Trajectory tracking control of an autonomous underwater vehicle using Lyapunov-based model predictive control. IEEE Trans. Ind. Electron. 65 (7), 5796–5805.

Smallwood, D.A., Whitcomb, L.L., 2004. Model-based dynamic positioning of underwater robotic vehicles: theory and experiment. IEEE J. Ocean. Eng. 29 (1), 169–186.

Sun, B., Zhu, D., Yang, S.X., 2018. An optimized Fuzzy control algorithm for three-dimensional AUV path planning. Int. J. Fuzzy Syst. 20 (2), 597–610.

Teo, K., An, E., Beaujean, P.P.J., 2012. A robust Fuzzy autonomous underwater vehicle (AUV) docking approach for unknown current disturbances. IEEE J. Ocean. Eng. 37 (2), 143–155.

Wang, C., Liu, X., Yang, X., Hu, F., Jiang, A., Yang, C., 2018. Trajectory tracking of an omni-directional wheeled mobile robot using a model predictive control strategy. Appl. Sci. 8 (2), 231–245.

Wang, Z., Lu, R., Wang, H., 2017. Finite-time trajectory tracking control of a class of nonlinear discrete-time systems. IEEE Trans. Syst. Man Cybern. 47 (7), 1679–1687.

Xiang, X., Jouvencel, B., Parodi, O., 2010. Coordinated formation control of multiple autonomous underwater vehicles for pipeline inspection. Int. J. Adv. Robot. Syst. 7 (1), 75–84.

Xiang, X., Lapierre, L., Jouvencel, B., 2015. Smooth transition of AUV motion control: From fully-actuated to under-actuated configuration. Robot. Auton. Syst. 67, 14–22.

Xiang, X., Yu, C., Lapierre, L., Zhang, J., Zhang, Q., 2017. Survey on Fuzzy-logic-based guidance and control of marine surface vehicles and underwater vehicles. Int. J. Fuzzy Syst. 20 (2), 572–586.

Xu, J., Wang, M., Qiao, L., 2014. Backstepping-based controller for three-dimensional trajectory tracking of underactuated unmanned underwater vehicles. Control Theory Appl. 31 (11), 1589–1596.

Xu, J., Wang, M., Qiao, L., 2015. Dynamical sliding mode control for the trajectory tracking of underactuated unmanned underwater vehicles. Ocean Eng. 105, 54–63.

Ye, L., Cong, W., Qi, W., Chen, P., Jiang, Y., Li, Y., 2015. Study of 3 dimension trajectory tracking of underactuated autonomous underwater vehicle. Ocean Eng. 105, 270–274.

Zhang, F., Fratantoni, D., Paley, D., Lund, J., Leonard, N., 2007. Control of coordinated patterns for ocean sampling. Internat. J. Control 80 (7), 1186–1199.

Zhang, F., Marani, G., Smith, R.N., Choi, H.T., 2015. Future trends in marine robotics. IEEE Robot. Autom. Mag. 22 (1), 14–122.

Zhu, D., Cao, X., Sun, B., Luo, C., 2018. Biologically inspired self-organizing map applied to task assignment and path planning of an AUV system. IEEE Trans. Cogn. Dev. Syst. 10 (2), 304–313.